Performance of Medium-Voltage DC-Bus PV System Architecture Utilizing High-Gain DC–DC Converter

Hyuntae Choi, *Student Member, IEEE*, Mihai Ciobotaru, *Senior Member, IEEE*, Minsoo Jang, *Member, IEEE*, and Vassilios G. Agelidis, *Senior Member, IEEE*

***Abstract*—The number of large-scale solar photovoltaic (PV) systems continues to increase, while the size of the largest systems has already reached several hundred megawatts. This trend will challenge existing PV system architectures and will require new PV system architectures with higher power ratings and higher voltage levels at the point of common coupling (PCC). This paper reports a medium-voltage (MV) dc-bus PV system architecture based on a high-gain soft-switched interleaved boost (SSIB) dc–dc converter. The interleaved characteristic increases the flexibility of the converter, allowing for either a higher voltage and/or current rating, thus increasing the power rating of the converter. The high-gain capability of the SSIB converter allows it to be connected directly to an MV dc bus. This will facilitate direct connection of a PV system to an MV ac grid (i.e., 20 kV) using only one step-up transformer. Simulation and experimental results are presented to verify the operation of the SSIB converter and to confirm the steady-state and dynamic performance of the proposed PV system architecture.**

***Index Terms*—DC–DC power converters, large-scale systems, photovoltaic (PV) systems, power conversion.**

I. Introduction

OVER THE PAST decade, the interest in grid-connected solar photovoltaic (PV) systems has increased significantly [1]–[3]. In 2013, more than 37 GW of solar power generation capacity was installed around the world, and global cumulative PV installed capacity reached 136.7 GW [4]. This rapid expansion of capacity is predominantly achieved through large-scale PV systems, which range in capacity from 200 kW up to several hundred MW [5]. Large-scale PV systems are becoming more commercially attractive than smaller systems, since they are capable of delivering further reductions in the system's cost-per-watt ratio. Hence, it is expected that the capacity of new PV systems will continue to grow. This trend will require PV system architectures that incorporate converters with higher power ratings and a higher voltage level at the point of common coupling (PCC), which in turn will require higher ratio transformers or more transformation stages for connection to a medium-voltage (MV) or high-voltage (HV) electricity grid.

Currently, large-scale PV systems interface to the grid via central or multistring inverter configurations [6]. Fig. 1(a) presents the central inverter configuration, which is very commonly used due to its simplicity and low installation cost. Nevertheless, mismatch power losses from the limitation of single maximum power point tracking (MPPT), particularly under partial shading conditions, and the power losses from the reverse-current blocking diodes degrade the efficiency of this PV configuration [7]. The multistring configuration introduces dc–dc converters between the PV array and the inverter, as shown in Fig. 1(b) and (c). Most commercial multistring PV inverters place dc–dc converters inside the same casing, as shown in Fig. 1(c), and their power range is between 5 and 20 kW [8]–[10]. Fig. 1(b) presents a multistring configuration for large-scale PV systems [11]. The additional power converter allows each PV array to be operated at its maximum power point (MPP), which greatly increases the overall MPPT efficiency. A higher MPPT efficiency will outweigh the increased cost of the additional power conversion stage. A central PV inverter configuration for direct medium-voltage connection has been commercialized [12], as shown in Fig. 1(d). Although the efficiency is increased and overall costs are lowered by achieving MV grid integration with only one step-up transformer, the inverter includes an MV-level transformer with a high turns ratio.

Large-scale PV system architectures with reduced transformer stages can be realized by using high-gain dc–dc converters. Recently, a number of papers regarding high-gain dc–dc converters have been published [13]–[28]. To increase the voltage conversion ratio, switched-capacitor converters have been proposed in [13]–[16]. The switched-capacitor technology increases the voltage conversion ratio and decreases the voltage stress of the devices. Although the switched-capacitor technique does not involve magnetic components, the power switches suffer high transient currents and many components are required to achieve high gain, thus increasing the circuit complexity and associated cost. Coupled-inductor converters are an alternative solution for obtaining high gain [17]–[21]. Despite the considerably high gain of such converters, achieved by the coupled inductor acting as a transformer, significant energy losses of the leakage inductance degrade the efficiency of the converter. Moreover, the converter topology and placement of components are constrained, leading to a relatively complex design. Interleaved coupled-inductor converters have been proposed in [22]–[26], and simplified interleaved

Manuscript received August 15, 2014; revised November 27, 2014; accepted December 13, 2014. Date of publication February 03, 2015; date of current version March 18, 2015. This paper was presented at the IEEE International Symposium on Industrial Electronics (ISIE 2012), Hangzhou, China, June 2012. Paper no. TSTE-00414-2014.

The authors are with the Australian Energy Research Institute, School of Electrical Engineering and Telecommunications, University of New South Wales, Sydney, N.S.W. 2052, Australia (e-mail: hyuntae@ieee.org; mihai.ciobotaru@unsw.edu.au; minsoo@unsw.edu.au; vassilios.agelidis@unsw.edu.au).

Color versions of one or more of the figures in this paper are available online at http://ieeexplore.ieee.org.

Digital Object Identifier 10.1109/TSTE.2014.2382690

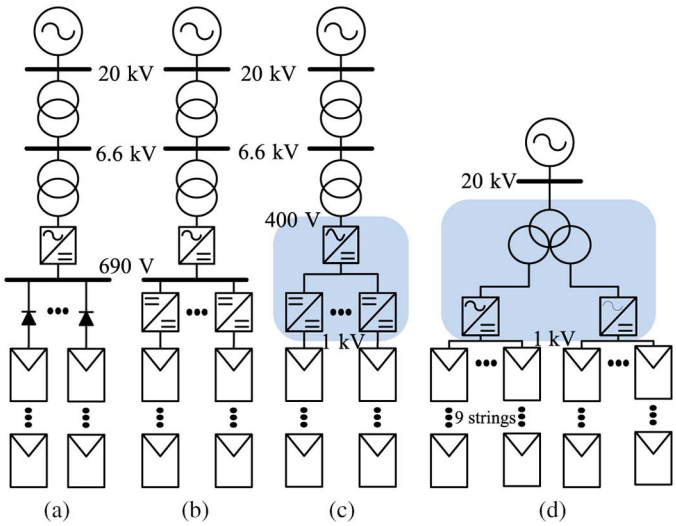

Fig. 1. Large-scale PV system configurations. (a) Central inverter configuration. (b) Multistring inverter configuration. (c) Commercialized multistring inverter configuration. (d) Central inverter configuration with only one step-up transformer.

coupled-inductor converter topologies were introduced in [27] and [28]. The interleaved configuration supports an increase of the converter power rating, but the disadvantages of the coupled inductor remain an issue. A soft-switched boost (SSB) converter was proposed in [29] and [30]. The converter achieves high gain without using a switched capacitor or coupled inductor. Moreover, Park and Choi [29] present conceptual circuit diagrams of the interleaved configurations. However, detailed analysis and implementation of the interleaved configuration have not been reported yet in the technical literature.

A PV system architecture based on a high-gain soft-switched interleaved boost (SSIB) converter was previously introduced in [31]. This paper expands existing work presented at International Symposium on Industrial Electronics 2012 (ISIE 2012) [31] by providing a more detailed topology selection and design of the SSIB converter, the experimental implementation of the proposed PV system architecture, and the experimental validation through a quantitative comparison between the simulation and experimental results.

This paper is organized as follows: Section II describes the MV dc-bus PV system architecture. In Section III, simulation results are presented to document the steady-state and dynamic performance of the large-scale PV system architecture. Experimental verification of the MV dc-bus PV system architecture using SSIB converters is presented in Section IV. Finally, the conclusion is summarized in Section V.

II. MV DC-BUS System Architecture

A schematic view of the MV dc-bus PV system architecture based on SSIB converters is shown in Fig. 2. The PV system architecture contains three identical PV arrays, one step-up transformer and two power conversion stages: a dc–dc stage using SSIB converters and a dc–ac stage using a voltage source converter (VSC). The PV array contains several parallel connected PV strings consisting of many PV panels connected in series. A conventional inverter consisting of

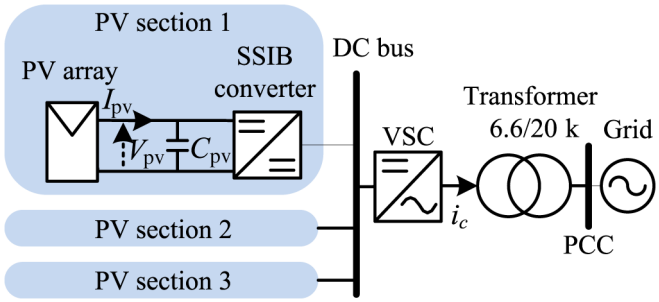

Fig. 2. Large-scale PV system architecture.

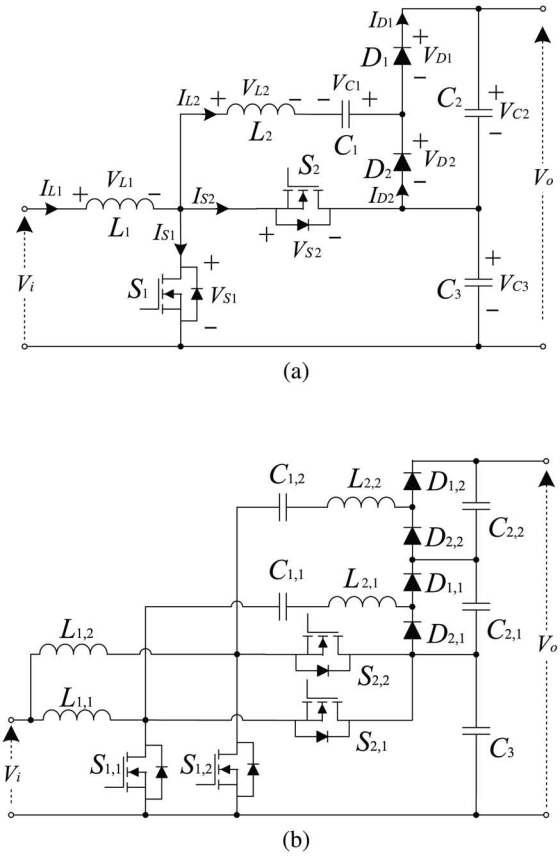

Fig. 3. Converter topology. (a) SSB converter. (b) SSIB converter ($N = 2$, $P = 1$).

a VSC with sinusoidal pulsewidth modulation (PWM) and a delta-wye ($\Delta - Y$) MV-level transformer is considered in this paper. Three identical SSIB converters transfer the power generated by each PV array to a common MV dc bus. At the same time, each SSIB converter controls the output voltage of their associated PV array. The voltage of the MV dc bus is controlled by the inverter, thus transferring all the available power to the electricity grid via an MV-level transformer. A more detailed description of the system components is given in Section III.

A. SSIB Converter

The SSB converter topology and the conceptual idea of interleaving were proposed in [29]. The circuit configuration of the SSB converter is shown in Fig. 3(a). The converter substitutes the rectifier diode of a conventional boost converter

with a switch (S_2) and introduces an auxiliary circuit, which is composed of an inductor (L_2), a capacitor (C_1), and a voltage-doubler circuit. The voltage-doubler circuit comprises two diodes (D_1 and D_2) and a capacitor (C_2). The auxiliary circuit allows the converter to have a higher voltage gain than the conventional boost converter, and helps to achieve zero voltage switching (ZVS) of both the lower switch (S_1) and upper switch (S_2). Additionally, zero current switching (ZCS) of the voltage-doubler diodes (D_1 and D_2) is achieved by discontinuous conduction mode (DCM) operation of L_2.

The SSB converter configuration can be extended to an interleaved converter, where a number of converters are connected in parallel and/or in series (N, number of series connected voltage doublers, P, number of parallel connected diode legs in voltage doubler). A higher voltage gain can be achieved by increasing N, while an elevated current rating of the converter can be accomplished by increasing P. At the same time, the input current ripple is reduced as N and P increase. In this paper, an $N = 2$, $P = 1$ SSIB converter is considered for connecting a PV array to an MV-level grid. The circuit diagram is shown in Fig. 3(b).

Based on the analysis of the single-phase converter ($N = 1$, $P = 1$) reported in [29], the characteristics of the interleaved converter ($N = 2$, $P = 1$) are derived. The ideal output voltage ($V_{\text{o\_ideal}}$) is given by

$$V_{\text{o\_ideal}} = \frac{N+1}{1-D}V_i = \frac{3}{1-D}V_i. \tag{1}$$

However, the presence of a voltage peak at $L_{2n,p}$ creates a duty-cycle loss (D_{loss}), which is the duration ratio of the voltage peak at L_2 to switching period T_s [see Fig. 11(d)]. This duty loss leads to a voltage drop at $C_{2,1}$ and $C_{2,2}$. The actual output voltage (V_o) can be expressed as

$$V_o = \frac{3}{1-(D-D_{\text{loss}})}V_i. \tag{2}$$

The difference between the input inductor current $I_{L1,n}$ and the auxiliary inductor current $I_{L2,n}$ is the main independent variable for ZVS operation of switches $S_{1,n}$ and $S_{2,n}$. To ensure ZVS operation of $S_{1,n}$, the following condition should be satisfied [29]:

$$\frac{1}{2}\left(L_{2,n}I_{L_{2,n},+pk}^2 + L_{1,n}I_{L_{1,n},\min}^2\right) > \frac{1}{2}\left(C_{S_{1,n}} + C_{S_{2,n}}\right)\left(\frac{V_i}{1-D}\right)^2 \tag{3}$$

where $C_{S1,n}$ and $C_{S2,n}$ are the drain–source capacitances of $S_{1,n}$ and $S_{2,n}$, respectively; $I_{L2,n,+pk}$ is the positive peak value of $I_{L2,n}$, and $I_{L1,n,\min}$ is the minimum value of $I_{L1,n}$. The ZVS operation of $S_{2,n}$ is achieved when the following condition is satisfied [29]:

$$\frac{1}{2}\left(L_{1,n}I_{L_{1,n},\max}^2 + L_{2,n}I_{L_{2,n},-pk}^2\right) > \frac{1}{2}\left(C_{S_{1,n}} + C_{S_{2,n}}\right)\left(\frac{V_i}{1-D}\right)^2 \tag{4}$$

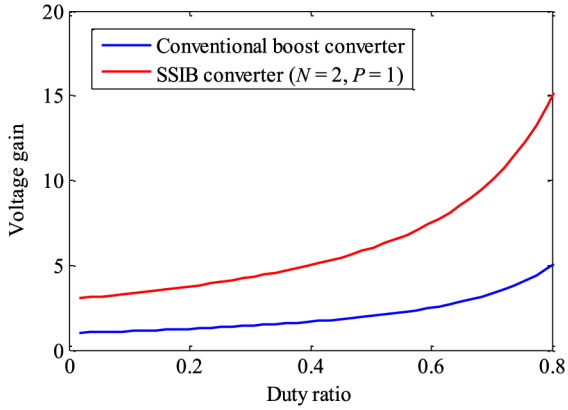

Fig. 4. Voltage gains of SSIB converter ($N = 2$, $P = 1$) and conventional boost converter.

where $I_{L2,n,-pk}$ is the negative peak value of $I_{L2,n}$ and $I_{L1,n,\max}$ is the maximum value of $I_{L1,n}$.

Although (3) and (4) could be satisfied with small $L_{1,n}$ and large $L_{2,n}$, reducing $L_{1,n}$ will increase the input current ripple, and increasing $L_{2,n}$ will elevate the duty-cycle loss, which will affect the voltage gain of the converter.

The relationship between the voltage gain and duty ratio of a conventional boost converter and $N = 2$, $P = 1$ SSIB converter is illustrated in Fig. 4. The voltage gain of the SSIB converter is three times higher than that of the conventional boost converter. However, N is limited due to the voltage rating of the auxiliary capacitor, which can be derived as

$$V_{C_{1,k}} = V_{C_3} + (k-1)\frac{V_o}{1+N} - \sum_{m=1}^{k-1} V_{\text{loss},C2\,m} \tag{5}$$

where $k = 1, 2, \ldots, N$ and $V_{\text{loss},C2,m}$ is the voltage drop on $C_{2,1}$ and $C_{2,2}$. The voltage rating of each auxiliary capacitor is different and the uppermost auxiliary capacitor $C_{1,N}$ has the highest voltage rating, as follows:

$$V_{C_{1,N}} = V_o - V_{C_{2,N}}. \tag{6}$$

The interleaved asymmetrical PWM switching technique is applied to the converter, which results in asymmetrical ripples in the input inductor current. This leads to smaller input current ripples (PV current), thus resulting in better MPPT performance. Fig. 5 shows the relationship between the input current ripple and the duty ratio of the $N = 2$, $P = 1$ SSIB converter and the conventional boost converter. Based on the input current equation of interleaved boost converter [32], the input current ripple of the SSIB converter can be expressed as

$$\begin{cases} \Delta i_{i,n} = \sqrt{2D(1-2D)}\dfrac{V_i}{L_{1,n}\cdot f_s}, & (D \le 0.5) \\ \Delta i_{i,n} = \sqrt{2(1-D)\left[1-2(1-D)\right]}\dfrac{V_i}{L_{1,n}\cdot f_s}, & (D > 0.5). \end{cases} \tag{7}$$

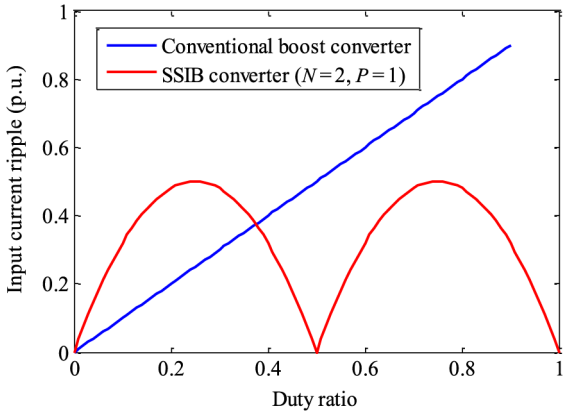

Fig. 5. Input current ripple of SSIB converter ($N = 2$, $P = 1$) and conventional boost converter.

TABLE I
VOLTAGE GAIN AND DUTY CYCLE OF CONVERTER WITH DIFFERENT VALUES OF N

		$N=1$	$N=2$	$N=3$
Voltage gain	Min MPP (400 V)	18.75		
	Max MPP (820 V)	9.14		
Duty cycle	Min MPP (400 V)	0.893	0.84	0.786
	Max MPP (820 V)	0.781	0.671	0.562

B. SSIB Converter for PV Application

When connecting a large-scale PV system (MW level or higher) to the MV or HV electricity grid, multiple transformer stages are usually required. This is because the maximum allowed dc output voltage of a PV string is 1000 V (600 V in North America) [33], and the voltage at the PCC has to be 20 kV or above. Consequently, most MV or HV grid-connected large-scale PV systems have two transformer stages, as shown in Fig. 1(a) and (b). To connect a large PV system to an MV grid through only one step-up transformer, the SSIB converter needs to provide a voltage gain that can boost the minimum MPP voltage to the voltage of the MV dc bus, in this case 7.5 kV.

1) Converter Configuration: Greater values of N allow the converter to operate with a lower duty cycle. At the same time, the input current ripple is reduced by a factor of $1/N$, and can be reduced further depending on the duty cycle. The reduced input current ripple results in better MPPT performance. However, N is limited due to the voltage rating of the auxiliary capacitor. As described in (5), the voltage rating of the uppermost auxiliary capacitor increases with increasing N. Therefore, N should be properly chosen considering a tradeoff between converter operating duty cycle, input current ripple, and voltage rating of the auxiliary capacitor. The required voltage gain and duty cycle of an SSIB converter with different values of N are summarized in Table I.

Choosing a proper value of P is also an important factor when using the SSIB converter for PV system applications. The current rating of the converter is increased by a factor of P, thus increasing the power rating of the converter. Moreover, the input current ripple is decreased by a factor of $1/P$, which can increase the MPPT efficiency. Although increasing P provides such advantages, it also involves increased circuit complexity and higher component count. The relationship of component count, input current ripple, and power rating with respect to P is summarized in Table II. When selecting a proper P, the converter power rating should be considered at first, and then the other parameters, such as current ripple size and component count.

TABLE II
COMPONENT COUNT, INPUT CURRENT RIPPLE, AND POWER RATING OF CONVERTER WITH DIFFERENT VALUES OF P

	$P=1$	$P=2$	$P=3$	$p=1, 2, \ldots, P$
Component count	9	16	24	$9p-2(p-1)$
Input current ripple	ΔI	$\Delta I/2$	$\Delta I/3$	$\Delta I/p$
Converter power rating	P_c	$2P_c$	$3P_c$	pP_c

Based on Tables I, II, and the other characteristics of an SSIB converter described in Section II-A, $N = 2$ and $P = 1$ SSIB converter was selected for the PV system application.

2) Converter Design: In this paper, the SSIB converter is designed for a PV application. The input voltage range and the required output voltage of the SSIB converter are determined by the characteristics of the PV system. Output capacitors (C_3, $C_{2,1}$, and $C_{2,2}$) are chosen based on (1) and N with respect to the voltage rating. Since the required output voltage is 7.5 kV and $N = 2$, the output capacitor voltage rating is 2.5 kV. A value of 250 μF is selected for the output capacitors considering a maximum of 5% voltage ripple. The voltage rating of auxiliary capacitors ($C_{1,1}$ and $C_{1,2}$) is calculated using (5) and (6). A value of 50 μF is selected for the auxiliary capacitors considering a maximum of 5% voltage ripple. The input inductance (L_1) is selected based on the maximum allowed current ripple using (7). After determining L_1, the minimum auxiliary inductance (L_2) for ensuring ZVS operation is calculated based on (3) and (4). A value of 1.1 mH is selected for L_1 considering 30% current ripple and 100 μH for L_2.

3) Converter Control: The control of an SSIB converter based on an MPPT algorithm is another important issue to be considered when applying the converter to PV application. Based on the incremental conductance method [34] [Fig. 6(b)], the SSIB converter maintains the PV array voltage at the MPP. The control block diagram is shown in Fig. 6(a). The MPPT method adjusts the PV array voltage to the MPP voltage by comparing the instantaneous conductance ($I_{\rm pv}/V_{\rm pv}$) to the incremental conductance ($dI_{\rm pv}/dV_{\rm pv}$) [34]. The tracking speed is determined by the increment size (inc). Although fast tracking can be achieved with large increments, the PV array might not operate at the MPP but instead oscillate around the MPP, which would degrade the controller performance. Therefore, the increment size should be properly chosen considering a

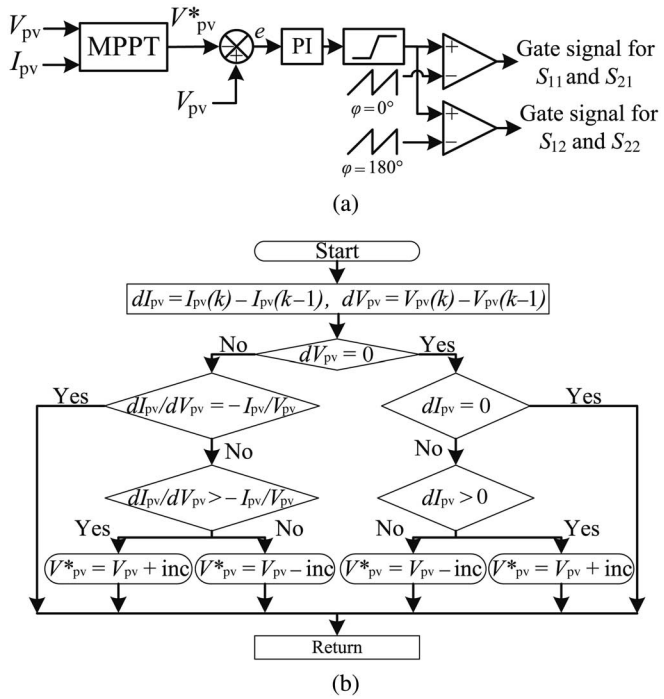

Fig. 6. Control block diagram. (a) $N = 2$, $P = 1$ SSIB converter control loop. (b) Incremental conductance MPPT algorithm [31].

tradeoff between the tracking speed and the performance of the controller [34], [35]. The MPPT algorithm generates the reference voltage $V^*_{\rm pv}$ and the PV array voltage ($V_{\rm pv}$) is regulated at $V^*_{\rm pv}$ by a proportional-integral (PI) controller. The transfer function of conventional PI compensator can be expressed as

$$G(s) = k_p + \frac{k_i}{s} \tag{8}$$

where k_p is the proportional gain and k_i is the integral gain of PI controller. The voltage error [e in Fig. 6(a)] is defined as

$$E(s) = -V^*_{\rm pv}(s) + V_{\rm pv}(s). \tag{9}$$

The closed-loop transfer function of the control system can be expressed as [36], [37]

$$T(s) = \frac{V_{\rm pv}(s)}{V^*_{\rm pv}(s)} = \frac{k_p s + k_i}{C_{\rm pv} s^2 + k_p s + k_i} \tag{10}$$

where $C_{\rm pv}$ is the PV array output capacitor shown in Fig. 2. The damping ratio $\zeta = k_p/(2C_{\rm pv}\sqrt{k_i/C_{\rm pv}})$ and natural frequency $\omega_n^2 = k_i/C_{\rm pv}$. Thus, the parameters of the PI controller can be given as follows:

$$\begin{aligned} k_p &= 2C_{\rm pv}\zeta\omega_n \\ k_i &= C_{\rm pv}\omega_n^2. \end{aligned} \tag{11}$$

The selected values for k_p and k_i are $1.5\mathrm{e}^{-3}$ and 4.7, respectively. The same parameter values are used for experimental verification.

TABLE III
SPECIFICATIONS FOR THE PV SYSTEM

PV array	
Array configuration	Series: 45 ($V_{\rm MPP}$: 794.97 V) Parallel: 34 ($I_{\rm MPP}$: 125.12 A)
Maximum power rate $P_{\rm MPP}$	99.5 kW
SSIB converter (N = 2, P = 1)	
Topology	N: 2 P: 1
Switching frequency $f_{\rm S\text{-}dc}$	80 kHz
Input inductor L_1	1.1 mH
Auxiliary inductor L_2	100 μH
Auxiliary capacitor C_1	50 μF
Output capacitors C_2 and C_3	250 μF
Other parameter	
Dc bus voltage $V_{\rm dc}$	7.5 kV
Grid voltage	20 kV
VSC switching frequency $f_{\rm S\text{-}VSC}$	2 kHz
Utility frequency $f_{\rm S}$	50 Hz
Transformer turns ratio	$N1$:$N2$ = 6.6 k:22 k (1:3.33)

III. SIMULATION RESULTS

This section presents the simulation results of the MV dc-bus PV system architecture. To validate the overall performance of the PV system, a 300-kW PV system was simulated using MATLAB/Simulink and PLECS [38], [39]. For simplicity purpose, three sections (100 kW each) of the large-scale PV system were considered, as shown in Fig. 2, taking into account that the simulation model of the power converter has been built using switching models. Additionally, losses were neglected for all simulation results. Each PV string contains a total of 45 PV panels, and the PV array section consists of 34 PV strings connected in parallel, reaching 99.5 kW. The parameters of the proposed PV system are given in Table III.

The synchronous reference frame technique has been used to control the VSC [40]. As shown in Fig. 7, the VSC control block diagram consists of an outer control loop and an inner current control loop for each d- and q-axis. The outer control loops regulate the dc-bus voltage and the reactive power. The inner control loops regulate the active (i_{cd}) and reactive current (i_{cq}) by using PI controllers. Synchronization between the converter and the grid is achieved by using a three-phase phase-locked-loop (PLL) technique [41], [42].

The performance of the MPPT controller using the SSIB converter is shown in Fig. 8. Starting at the open circuit voltage of the PV array, the converter adjusts the PV array voltage toward the MPP voltage based on the MPPT controller shown in Fig. 6. As observed in Fig. 8, the MPPT controller maintains the PV array voltage at the MPP voltage with small variation.

The steady-state and dynamic performance of the PV system were tested with a trapezoidal solar irradiation profile [36], [37], [43], as shown in Fig. 9(a). A trapezoidal solar irradiation profile has been chosen for the following reasons. For small intervals of time, the solar irradiation can be approximated with

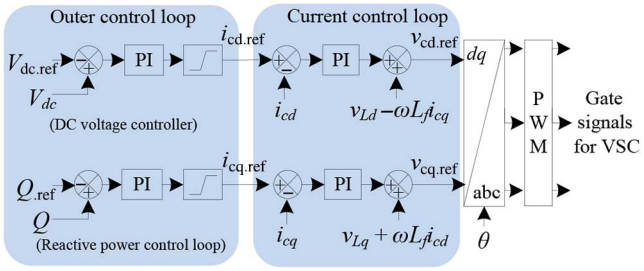

Fig. 7. VSC control block diagram.

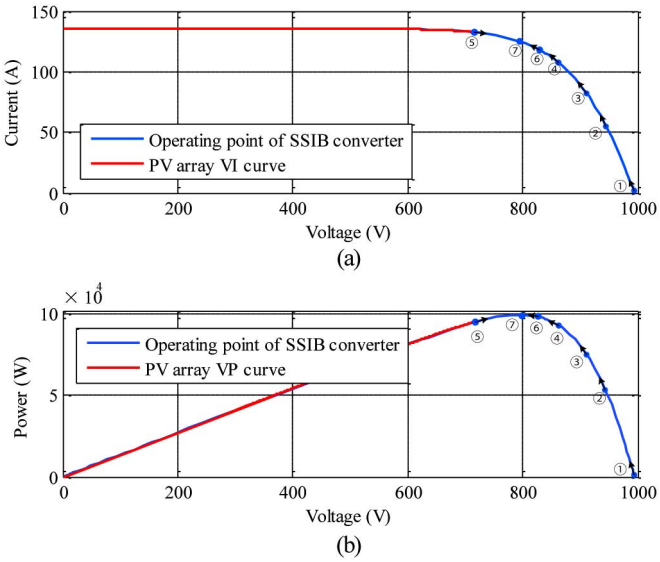

Fig. 8. Simulation results. (a) *V–I* curve of PV array and operating point of SSIB converter. (b) *V–P* curve of PV array and operating point of SSIB converter.

a linear slope/ramp. The inclination of the slope is chosen in accordance with the worst case scenario, when the solar irradiation changes rapidly due to fast moving low-altitude clouds. The flat part of the trapezoidal profile is considered as the steady-state condition, while the positive and negative slopes represent the dynamic conditions. The irradiation increases linearly from 300 to 1000 W/m^2 over 1 s, remains steady at 1000 W/m^2 for 1 s, then decreased linearly to 300 W/m^2 over 1 s. The currents and voltages of the PV arrays are shown in Fig. 9(b) and (c), respectively. These show that the MPP current follows the solar irradiation profile, as it is directly affected by the solar irradiation, while the change in MPP voltage is relatively small. The MPPT algorithm ensures that the PV array is maintained at close to its MPP under rapidly changing solar irradiation. The dc-bus voltage and active/reactive power are shown in Fig. 9(d) and (e), respectively. The active power follows the solar irradiation profile. The dc-bus voltage and the reactive power are regulated at their specified reference values, 7.5 kV and 0 var, respectively.

IV. Experimental Results

Due to laboratory limitations, both the rated voltage level and the current level of the PV system architecture have been scaled down by the factor of 10 for experimental verification

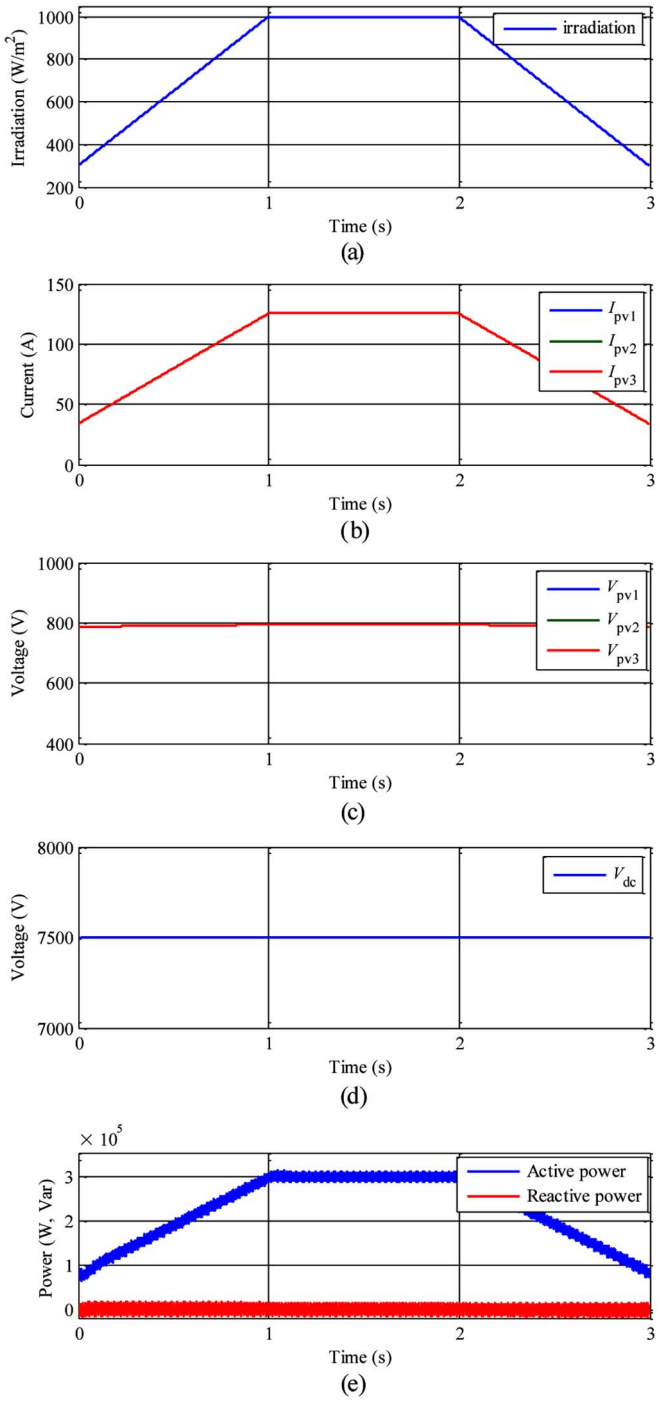

Fig. 9. Simulation results. (a) Solar irradiation. (b) PV array currents. (c) PV array voltages. (d) DC-bus voltage. (e) Active and reactive power.

and a single section of the PV array has been considered. A solar array simulator (Regatron TC.P.16.600.400.S, 600 V, 16 kW) was used for the PV array. To enhance the performance and accuracy of the power supply around the MPP, a linear postprocessor (Regatron TC.LIN.SER.26.1000.26) was added to the solar array simulator. The MV dc bus was emulated using two series-connected dc-grid simulators (Regatron TC.GSS.20.600.400S, 600 V, ±20 kW). Since the main scope of this paper is to assess the hardware performance of the SSIB converter, the grid connection of the SSIB converter was

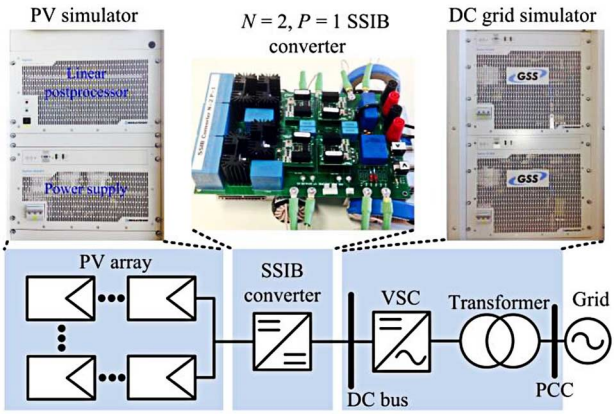

Fig. 10. Experimental setup of proposed PV system architecture.

TABLE IV
SPECIFICATIONS FOR THE EXPERIMENTAL SETUP

PV simulator	
Maximum power P_{MPP}	1 kW
MPP voltage V_{MPP}	80 V
MPP current I_{MPP}	12.5 A
Dc grid simulator	
Dc bus voltage V_{dc}	750 V
Ac grid voltage	240 V (3ϕ line to neutral)
Dc–dc converter	
Topology	N: 2 P: 1
Switching frequency $f_{S\text{-}DC}$	80 kHz
Input inductor L_1	110 µH
Auxiliary inductor L_2	10 µH
Auxiliary capacitor C_1	5 µF
Output capacitors C_2 and C_3	25 µF

emulated using dc-grid simulators. Fig. 10 shows the configuration of the experimental setup. The parameters of the experimental setup are summarized in Table IV.

A powder toroid core, model High Flux 58907A2, and type 2 litz wire (5×56, 38 AWG) were selected for inductor L_1 to reduce the core and copper losses. A High Flux toroid 58083A2 core and the same litz wire were chosen for inductor L_2. A $5-\mu$F, 1.1-kV film capacitor was chosen for C_1, and 25 µF, 650 V film capacitors were selected for both C_2 and C_3. The switches were CREE CMF20120D MOSFETs, and CREE C4D20120A Schottky diodes were used for diodes D_1 and D_2.

The steady-state operation results for $N = 2$, $P = 1$ SSIB converter are presented in Fig. 11. The input/output voltages and currents of the converter are shown in Fig. 11(a) and (b), respectively. The output voltage of the converter is 750 V, and thus the converter achieves a gain of 9.3 for a duty cycle of 0.71. Fig. 11(c) shows the input current I_{in} and input inductor currents $I_{L1,1}$ and $I_{L1,2}$. As mentioned before, asymmetrical ripples in $I_{L1,1}$ and $I_{L1,2}$ reduce the input current ripple.

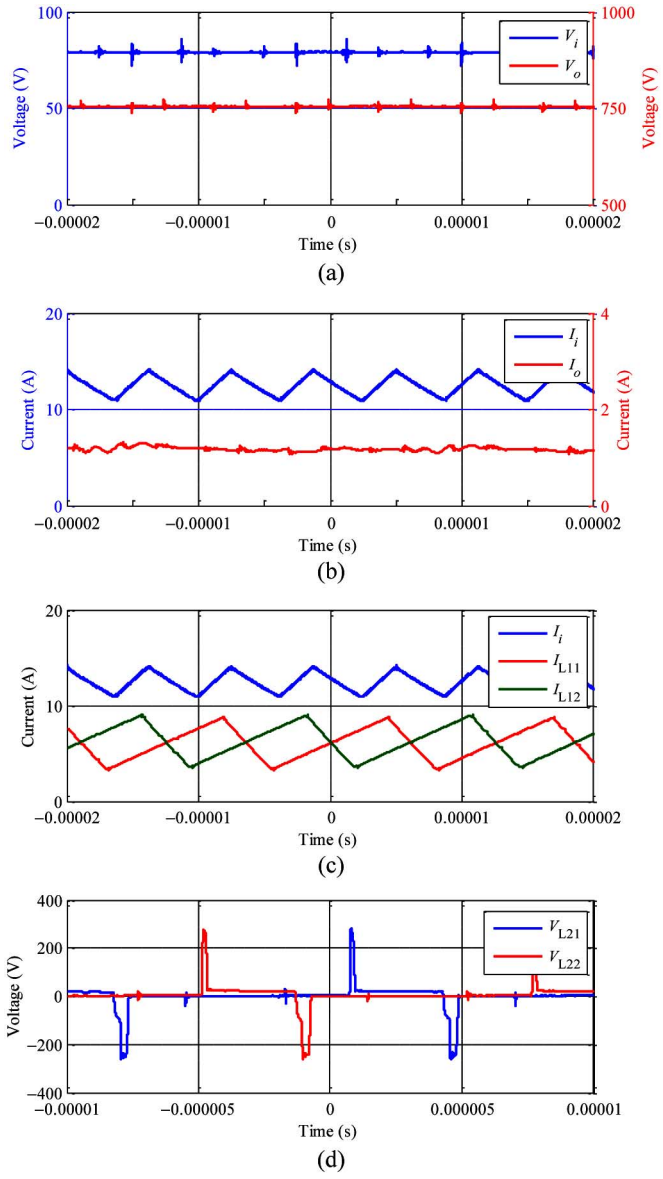

Fig. 11. Experimental results for $N = 2$, $P = 1$ SSIB converter. (a) Input and output voltages. (b) Input and output currents. (c) Input current I_i and currents of input inductors $L_{1,1}$ and $L_{1,2}$. (d) Voltages of auxiliary inductors $L_{2,1}$ and $L_{2,2}$.

Fig. 11(d) shows the voltage across the auxiliary inductors $L_{2,1}$ and $L_{2,2}$. The duration of the voltage peak at L_2 depends on the size of L_2; a higher inductance value leads to a longer duration voltage peak, which reduces the effective duty cycle.

Validation of the MPPT controller performance was made and the results are shown in Fig. 12. The MPPT controller was analyzed using a trapezoidal solar irradiation profile to verify the effect of rapidly changing irradiation conditions. As shown in Fig. 12(a), the irradiation increases linearly from 300 to 1000 W/m^2 over a period of 1 s, remains at 1000 W/m^2 for 1 s, and then decreases linearly back to 300 W/m^2 over a period of 1 s. An irradiation profile with relatively large variation was chosen to emphasize the effect of irradiation change on the MPP voltage. Fig. 12(b) shows the operating points of the PV array under rapidly changing irradiation, while several

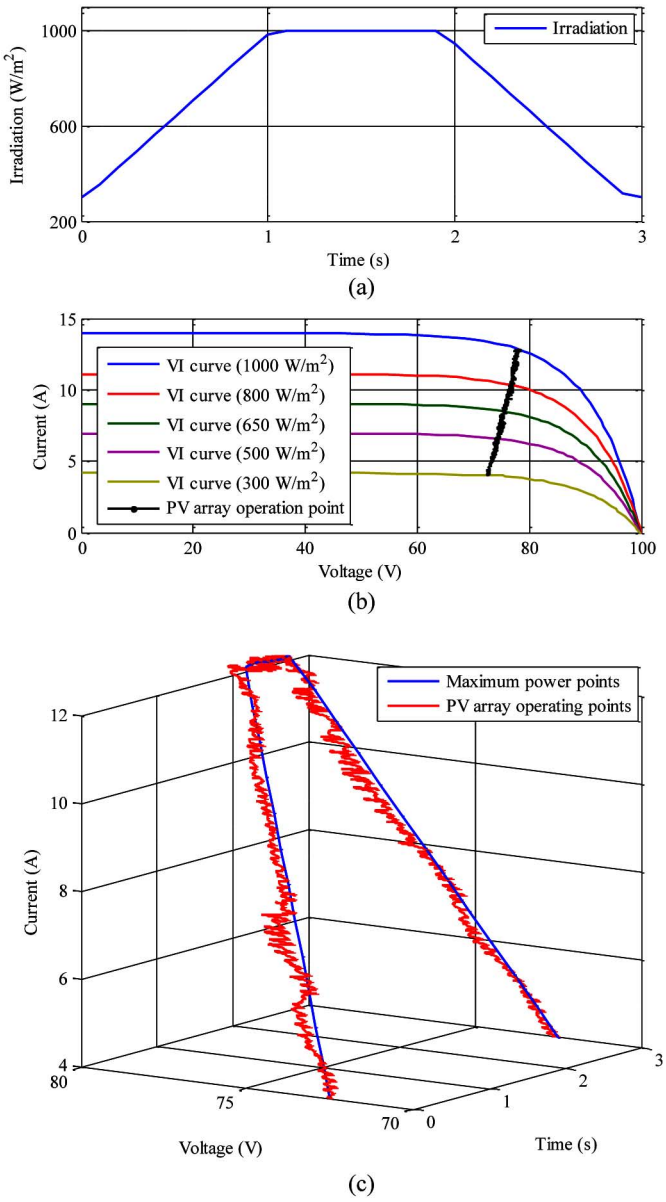

Fig. 12. MPPT controller performance. (a) Solar irradiation. (b) PV array operating point and VI curves with different level of solar irradiation. (c) PV array operating point and PV array MPP.

voltage-current (VI) curves are provided for reference. As can be seen, changes in the PV array current follow the irradiation profile, while changes in the PV array voltage are relatively small. To present more details of the MPPT controller operation, a three-dimensional curve along the dimensions of current, voltage and time, is presented in Fig. 12(c). This shows that the MPPT controller of the SSIB converter maintains the PV array operating point close to its MPP under either dynamic or steady-state solar irradiation condition.

Experimental results for the PV system architecture are shown in Fig. 13. Following the simulation study, the same solar irradiation profile [Fig. 13(a)] was considered to verify the steady-state and dynamic performance of the PV system based on SSIB converter. The parameters of experimental setup have been based on the parameters of the simulation model

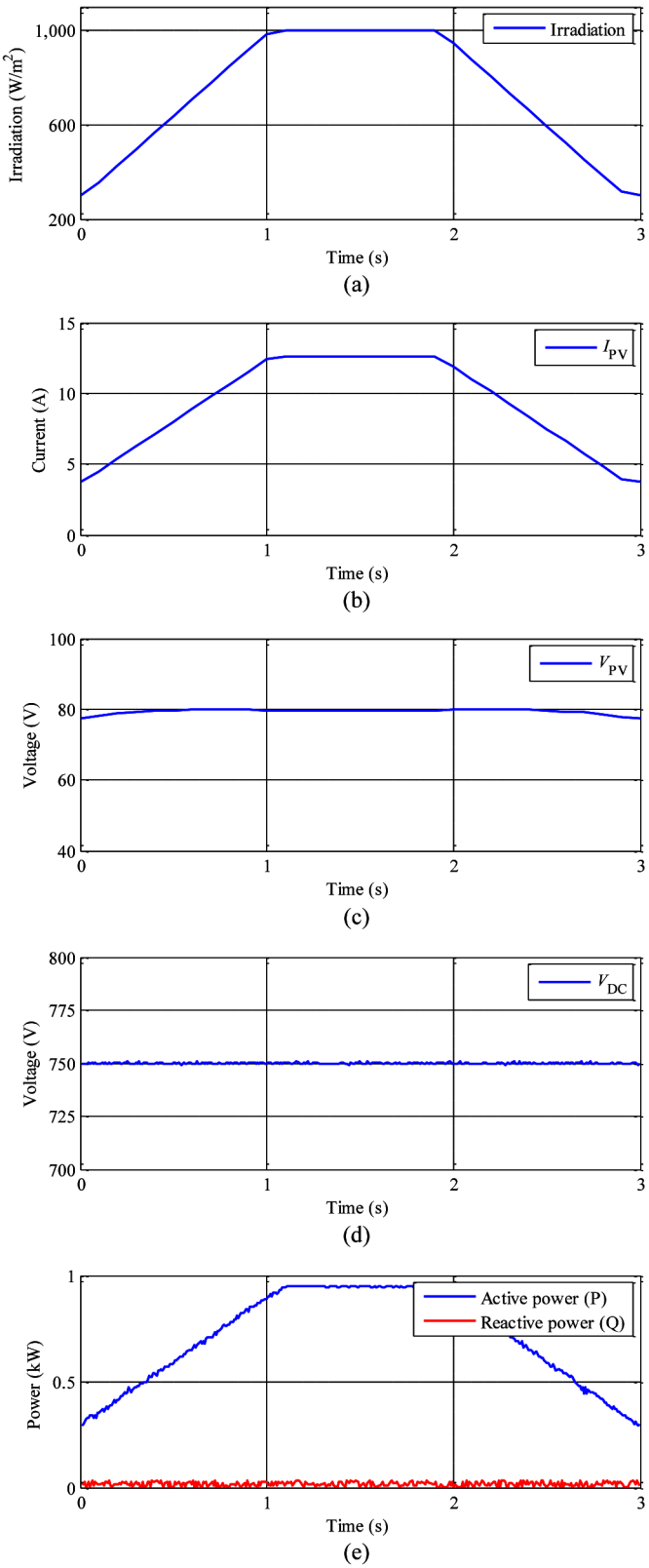

Fig. 13. Experimental results. (a) Solar irradiation. (b) PV array current. (c) PV array voltage. (d) DC-bus voltage. (e) Active and reactive power.

considering downscaling. In the experimental setup, the PV array is represented by a PV simulator, while the dc bus, inverter, and transformer were emulated by a dc-grid simulator.

Regardless of these differences, the simulation and experimental results were very similar. The current and voltage of the PV array are shown in Fig. 13(b) and (c), respectively. The performance of the MPPT controller under rapidly changing solar irradition is confirmed. The MPP current follows the solar irradiation profile, while the voltage changes little. The dc-bus voltage and the active and reactive power are shown in Fig. 13(d) and (e), respectively. The dc-bus voltage and reactive power are maintained at specified reference values, while the active power follows the solar irradiation profile.

V. Conclusion

An MV dc-bus PV system architecture based on a high-gain SSIB dc–dc converter has been reported in this paper. The MV ac grid connection of a PV system using only one step-up transformer has been achieved by introducing the SSIB converter. Simulation and experimental results verified both the steady-state and dynamic performance of the PV system architecture. The performance of the MPPT controller under rapidly changing solar irradiation conditions and the operation of the SSIB converter were confirmed. The $N = 2$, $P = 1$ SSIB converter achieved a voltage gain of 9.3 for a duty ratio of 0.71, thus proving that a PV system can achieve medium-voltage grid connection using only one step-up transformer.

References

[1] S. Kai, Z. Li, X. Yan, and J. M. Guerrero, "A distributed control strategy based on dc bus signaling for modular photovoltaic generation systems with battery energy storage," *IEEE Trans. Power Electron.*, vol. 26, no. 10, pp. 3032–3045, Oct. 2011.

[2] R. Yu, J. Kleissl, and S. Martinez, "Storage size determination for grid-connected photovoltaic systems," *IEEE Trans. Sustain. Energy*, vol. 4, no. 1, pp. 68–81, Jan. 2013.

[3] D. Velasco de la Fuente, C. L. T. Rodriguez, G. Garcera, E. Figueres, and R. O. Gonzalez, "Photovoltaic power system with battery backup with grid-connection and islanded operation capabilities," *IEEE Trans. Ind. Electron.*, vol. 60, no. 4, pp. 1571–1581, Apr. 2013.

[4] European Photovoltaic Industry Association (EPIA). (2013). *Market Report* [Online]. Available: www.epia.org

[5] T. Kerekes, E. Koutroulis, D. Sera, R. Teodorescu, and M. Katsanevakis, "An optimization method for designing large PV plants," *IEEE J. Photovoltaics*, vol. 3, no. 2, pp. 814–822, Apr. 2013.

[6] S. Rivera, W. Bin, S. Kouro, W. Hong, and Z. Donglai, "Cascaded H-bridge multilevel converter topology and three-phase balance control for large scale photovoltaic systems," in *Proc. IEEE Int. Symp. Power Electron. Distrib. Gener. Syst.*, 2012, pp. 690–697.

[7] S. B. Kjaer, J. K. Pedersen, and F. Blaabjerg, "A review of single-phase grid-connected inverters for photovoltaic modules," *IEEE Trans. Ind. Appl.*, vol. 41, no. 5, pp. 1292–1306, Sep./Oct. 2005.

[8] Danfoss. (2012). *TLX Inverter Series* [Online]. Available: http://www.danfoss.com/

[9] Ingeteam. (2011). *INGECON® SUN SMART (10–30 kW)* [Online]. Available: http://www.ingeteam.com/

[10] ABB. (2013). *Solar Inverters for Photovoltaic Systems* [Online]. Available: http://new.abb.com/solar

[11] S. Kouro *et al.*, "NPC multilevel multistring topology for large scale grid connected photovoltaic systems," in *Proc. IEEE Int. Symp. Power Electron. Distrib. Gener. Syst.*, 2010, pp. 400–405.

[12] SMA. (2012). *SUNNY CENTRAL for Direct Medium-Voltage Feed-in 500MV/630MV/ 800MV/1000MV/1250MV/1600MV–High-Performance Medium-Voltage Station in the Power Plant Class* [Online]. Available: www.sam.de/en

[13] D. Cao and F. Z. Peng, "Zero-current-switching multilevel modular switched-capacitor dc–dc converter," *IEEE Trans. Ind. Appl.*, vol. 46, no. 6, pp. 2536–2544, Nov./Dec. 2010.

[14] S. Xiong, S.-C. Tan, and S.-C. Wong, "Analysis and design of a high-voltage-gain hybrid switched-capacitor buck converter," *IEEE Trans. Circuits Syst. I, Reg. Papers*, vol. 59, no. 5, pp. 1132–1141, May 2012.

[15] L. Tsorng-Juu, C. Shih-Ming, Y. Lung-Sheng, C. Jiann-Fuh, and A. Ioinovici, "Ultra-large gain step-up switched-capacitor dc–dc converter with coupled inductor for alternative sources of energy," *IEEE Trans. Circuits Syst. I, Reg. Papers*, vol. 59, no. 4, pp. 864–874, Apr. 2012.

[16] Q. Wei *et al.*, "A switched-capacitor dc–dc converter with high voltage gain and reduced component rating and count," *IEEE Trans. Ind. Appl.*, vol. 48, no. 4, pp. 1397–1406, Jul./Aug. 2012.

[17] I. Laird and D. D. C. Lu, "High step-up dc/dc topology and MPPT algorithm for use with a thermoelectric generator," *IEEE Trans. Power Electron.*, vol. 28, no. 7, pp. 3147–3157, Jul. 2013.

[18] R. J. Wai, R. Y. Duan, and K. H. Jheng, "High-efficiency bidirectional dc–dc converter with high-voltage gain," *IET Power Electron.*, vol. 5, no. 2, pp. 173–184, Feb. 2012.

[19] D. Yan *et al.*, "Single-switch high step-up converters with built-in transformer voltage multiplier cell," *IEEE Trans. Power Electron.*, vol. 27, no. 8, pp. 3557–3567, Aug. 2012.

[20] Z. Yi, L. Wuhua, and H. Xiangning, "Single-phase improved active clamp coupled-inductor-based converter with extended voltage doubler cell," *IEEE Trans. Power Electron.*, vol. 27, no. 6, pp. 2869–2878, Jun. 2012.

[21] Y. Zhao, W. Li, Y. Deng, and X. He, "High step-up boost converter with passive lossless clamp circuit for non-isolated high step-up applications," *IET Power Electron.*, vol. 4, no. 8, pp. 851–859, Sep. 2011.

[22] S. V. Araujo, R. P. Torrico-Bascope, and G. V. Torrico-Bascope, "Highly efficient high step-up converter for fuel-cell power processing based on three-state commutation cell," *IEEE Trans. Ind. Electron.*, vol. 57, no. 6, pp. 1987–1997, Jun. 2010.

[23] S. Dwari and L. Parsa, "An efficient high-step-up interleaved dc–dc converter with a common active clamp," *IEEE Trans. Power Electron.*, vol. 26, no. 1, pp. 66–78, Jan. 2011.

[24] F. L. Tofoli, D. de Souza Oliveira, R. P. Torrico-Bascopeé, and Y. J. A. Alcazar, "Novel nonisolated high-voltage gain dc–dc converters based on 3SSC and VMC," *IEEE Trans. Power Electron.*, vol. 27, no. 9, pp. 3897–3907, Sep. 2012.

[25] L. Weichen, X. Xin, L. Chushan, L. Wuhua, and H. Xiangning, "Interleaved high step-up ZVT converter with built-in transformer voltage doubler cell for distributed PV generation system," *IEEE Trans. Power Electron.*, vol. 28, no. 1, pp. 300–313, Jan. 2013.

[26] L. Wuhua, Z. Yi, W. Jiande, and H. Xiangning, "Interleaved high step-up converter with winding-cross-coupled inductors and voltage multiplier cells," *IEEE Trans. Power Electron.*, vol. 27, no. 1, pp. 133–143, Jan. 2012.

[27] G. A. L. Henn, R. N. A. L. Silva, P. P. Praca, L. H. S. C. Barreto, and D. S. Oliveira, "Interleaved-boost converter with high voltage gain," *IEEE Trans. Power Electron.*, vol. 25, no. 11, pp. 2753–2761, Nov. 2010.

[28] L. Wuhua, Z. Yi, D. Yan, and H. Xiangning, "Interleaved converter with voltage multiplier cell for high step-up and high-efficiency conversion," *IEEE Trans. Power Electron.*, vol. 25, no. 9, pp. 2397–2408, Sep. 2010.

[29] S. Park and S. Choi, "Soft-switched CCM boost converters with high voltage gain for high-power applications," *IEEE Trans. Power Electron.*, vol. 25, no. 5, pp. 1211–1217, May 2010.

[30] M. Kwon, S. Oh, and S. Choi, "High gain soft-switching bidirectional dc–dc converter for eco-friendly vehicles," *IEEE Trans. Power Electron.*, vol. 29, no. 4, pp. 1659–1666, Apr. 2014.

[31] H. Choi, M. Ciobotaru, and V. G. Agelidis, "High gain dc/dc converter for the grid integration of large-scale PV systems," in *Proc. IEEE Int. Symp. Ind. Electron.*, 2012, pp. 1011–1016.

[32] H. B. Shin, J. G. Park, S. K. Chung, H. W. Lee, and T. A. Lipo, "Generalised steady-state analysis of multiphase interleaved boost converter with coupled inductors," in *Proc. IEE Electr. Power Appl.*, 2005, vol. 152, pp. 584–594.

[33] G. Ball, D. Brearley, and M. Hamon. (2013). 1000 Vdc utilization in nonresidential PV applications, *SOLARPRO*, vol. 6, no. 3, pp. 23–40 [Online]. Available: http://solarprofessional.com/

[34] T. Esram and P. L. Chapman, "Comparison of photovoltaic array maximum power point tracking techniques," *IEEE Trans. Energy Convers.*, vol. 22, no. 2, pp. 439–449, Jun. 2007.

[35] L. Fangrui, D. Shanxu, L. Fei, L. Bangyin, and K. Yong, "A variable step size INC MPPT method for PV systems," *IEEE Trans. Ind. Electron.*, vol. 55, no. 7, pp. 2622–2628, Jul. 2008.

[36] R. Kadri, J. P. Gaubert, and G. Champenois, "An improved maximum power point tracking for photovoltaic grid-connected inverter based on voltage-oriented control," *IEEE Trans. Ind. Electron.*, vol. 58, no. 1, pp. 66–75, Jan. 2011.

[37] E. Bianconi *et al.*, "A fast current-based MPPT technique employing sliding mode control," *IEEE Trans. Ind. Electron.*, vol. 60, no. 3, pp. 1168–1178, Mar. 2013.
[38] Mathworks. *MATLAB/Simulink*, version-2013b [Online]. Available: www.matlab.com
[39] Plexim Gmbh. *PLECS*, version-3.5.5 [Online]. Available: www.plexim.com
[40] M. P. Kazmierkowski, R. Krishnan, F. Blaabjerg, and J. D. Irwin, *Control in Power Electronics: Selected Problems*. Amsterdam, The Netherlands: Elsevier, 2002.
[41] H. Guan-Chyun and J. C. Hung, "Phase-locked loop techniques. A survey," *IEEE Trans. Ind. Electron.*, vol. 43, no. 6, pp. 609–615, Dec. 1996.
[42] S. K. Chung, "A phase tracking system for three phase utility interface inverters," *IEEE Trans. Power Electron.*, vol. 15, no. 3, pp. 431–438, May 2000.
[43] D. Sera, R. Teodorescu, J. Hantschel, and M. Knoll, "Optimized maximum power point tracker for fast-changing environmental conditions," *IEEE Trans. Ind. Electron.*, vol. 55, no. 7, pp. 2629–2637, Jul. 2008.

Hyuntae Choi (S'10) was born in Jeonju, Korea. He received the B.Eng. degree in electrical engineering from Chonbuk National University, Jeonju, Korea, in 2007, and the M.Eng. degree in electrical engineering and telecommunication from the University of New South Wales, Sydney, Australia, in 2012. He is currently working toward the Ph.D. degree in electrical engineering and telecommunication from the University of New South Wales.

Mihai Ciobotaru (S'04–M'08–SM'14) was born in Galati, Romania. He received the B.Sc. and M.Sc. degrees in electrical engineering from the University of Galati, Galati, Romania, in 2002 and 2003, respectively, and the Ph.D. degree in electrical engineering from the Institute of Energy Technology, Aalborg University, Aalborg, Denmark, in 2009.

From 2003 to 2004, he was an Associate Lecturer with the University of Galati. From 2007 to 2010, he was an Associate Research Fellow with the Institute of Energy Technology, Aalborg University. From 2010 to 2013, he was a Research Fellow with the School of Electrical Engineering and Telecommunications, University of New South Wales (UNSW), Sydney, Australia. Currently, he is a Senior Research Associate with the UNSW, performing his research activities under Australian Energy Research Institute. His research interests include grid integration of PV systems, control of grid connected converters, and power management of hybrid energy storage systems.

Minsoo Jang (S'09–M'13) received the B.S. and M.S. degrees in control and instrumentation engineering from Seoul National University of Technology (SNUT), Seoul, Korea, in 2001 and 2003, respectively, and the Ph.D. degree in electrical engineering and telecommunications from the University of New South Wales, Sydney, Australia, in 2012.

He joined the Australia Energy Research Institute, University of New South Wales, in 2012, where he is currently a Senior Research Associate. His research interests include power conversion technologies based on silicon carbide devices in renewable energy system, power quality, and digital power control.

Vassilios G. Agelidis (S'89–M'90–SM'00) was born in Serres, Greece. He received the B.Eng. degree in electrical engineering from Democritus University of Thrace, Thrace, Greece, in 1988, the M.S. degree in applied science from Concordia University, Montreal, QC, Canada, in 1992, and the Ph.D. degree in electrical engineering from Curtin University of Technology, Perth, Australia, in 1997.

From 1993 to 1999, he was with the School of Electrical and Computer Engineering, Curtin University. In 2000, he joined the University of Glasgow, Glasgow, U.K., as a Research Manager for the Glasgow-Strathclyde Centre for Economic Renewable Power Delivery. From January 2005 to December 2006, he was the Inaugural Chair of Power Engineering with the School of Electrical, Energy, and Process Engineering, Murdoch University, Perth, Australia. From December 2006 to June 2010, he was the Energy Australia Chair of Power Engineering with the University of Sydney. Currently, he is the Director of the Australian Energy Research Institute, University of New South Wales, Sydney, Australia. He has authored/coauthored several journal and conference papers as well as *Power Electronic Control in Electrical Systems* in 2002.

Dr. Agelidis was the Vice President Operations within the IEEE Power Electronics Society from 2006 to 2007. He was an Associate Editor of the IEEE POWER ELECTRONICS LETTERS from 2003 to 2005, and served as the Power Electronics Society (PELS) Chapter Development Committee Chair from 2003 to 2005. He was an AdCom Member of IEEE PELS from 2007 to 2009 and the Technical Chair of the 39th IEEE Annual Power Electronics Specialists Conference, Rhodes, Greece. He was the recipient the Advanced Research Fellowship from the United Kingdom's Engineering and Physical Sciences Research Council in 2004.